RSC Advances

This is an *Accepted Manuscript*, which has been through the Royal Society of Chemistry peer review process and has been accepted for publication.

Accepted Manuscripts are published online shortly after acceptance, before technical editing, formatting and proof reading. Using this free service, authors can make their results available to the community, in citable form, before we publish the edited article. This *Accepted Manuscript* will be replaced by the edited, formatted and paginated article as soon as this is available.

You can find more information about *Accepted Manuscripts* in the Information for Authors.

Please note that technical editing may introduce minor changes to the text and/or graphics, which may alter content. The journal's standard Terms & Conditions and the Ethical guidelines still apply. In no event shall the Royal Society of Chemistry be held responsible for any errors or omissions in this *Accepted Manuscript* or any consequences arising from the use of any information it contains.

ROYAL SOCIETY OF CHEMISTRY

www.rsc.org/advances

Pressure-induced hydrogen transfers and polymerization in crystalline furoxan

Qiong Wu, Weihua Zhu*, Heming Xiao

Institute for Computation in Molecular and Materials Science and School of Chemical Engineering, Nanjing University of Science and Technology, Nanjing 210094, China

Abstract: The structural transformations, electronic structure, elastic constants, and absorption properties of crystalline furoxan under hydrostatic compression of 0-160 GPa have been studied using density functional theory. The results show that furoxan (S1) undergoes a hydrogen transfer to form a new structure (named S2) with planar conformation approximately at 114-115 GPa first. Then, it goes through another hydrogen transfer to form the second new structure (named S3) with chair conformation at 124 GPa. Finally, it undergoes polymerization to form another new structure (named S4) with a trans-conformation at 136 GPa. An analysis of its band gaps and density of states under compression indicates that it changes from an insulator to a semiconductor in the pressure range 0-113 GPa. S2 and S4 have metallic properties, while S3 is an insulator. The calculated elastic constants show that the three new structures are mechanically stable. Its absorption spectra show that S2 has higher optical activity than S1. S3 has higher optical activity than S2 in far ultraviolet region, while S4 has weaker optical activity than S3 in this region. S4 and S2 have comparative optical activity.

Keywords density functional theory, structural transformations, electronic structure, elastic constants, absorption spectra

* Corresponding author. E-mail: zhuwh@njust.edu.cn

RSC Advances Accepted Manuscript

1 Introduction

Furoxan ($H_2C_2N_2O_2$) is an important synthetic precursor for technical and industrial materials [1-3] which was prepared from glyoxime by oxidizing with N_2O_4 in dichloromethane in 1994. [4] Therefore, studying its structure, properties, and synthesis is important to develop other electron-rich fuxoxan derivatives. Although some experimental [5, 6] and theoretical investigations [7-10] have been done on furoxan, many fundamental and practical problems are still not well understood because it possesses a complex chemical behavior. For instance, its behavior under high pressure is unknown until now.

Furoxan is an energetic compound and its derivatives like 7-amino-6-nitrobenzodifuroxan (ANBDF) [11] and benzotrifuroxan [12] have very good energetic properties and a potential use as high energy density materials. Both experimental studies [13-22] employing diamond-anvil-cell [15, 17-19] and theoretical studies [23-29] using DFT (density functional theory) on energetic molecular crystals like RDX (1,3,5-trinitro-1,3,5-triazinane) [15,16], FOX-7 (1,1-diamino-2,2-dintroethylene) [17], NM (nitromethane) [18], and TATB (triaminotrinitrobenzene) [19] reported that the pressure can produce an important influence on their crystal structure and properties like density, chemical reactivity, stability, and performance. The information under the pressure would be valuable and useful for the safe, effective, and cost-effective disposal of energetic materials. In addition, recent studies [23] reported that the crystal structure and properties of ANBDF changed obviously under high pressures. This may suggest that the effects of pressure on the crystal structure and properties of

RSC Advances Accepted Manuscript

furoxan and its derivatives are not negligible. Thus, a systematically study on the high-pressure behavior of furoxan not only is necessary for understanding its structure and properties clearly, but also could be helpful for well developing new furoxan-based energetic materials. In a word, there is a clear need to study the behavior of furoxan under high pressure.

It is still a challenging task for experiment measurements to investigate the microscopic properties of solid energetic materials under high pressure. An alternative approach is theoretical simulation, an effective way to model the physical and chemical properties of solid materials at the atomic level as a complement to experimental work. Recently, DFT with pseudopotentials and a plane-wave basis set has been applied to study the structures and properties of energetic solids successfully [24-29].

In this study, we performed periodic DFT calculations to study the effects of pressure on the crystal and molecular structure, electronic structure, elastic constants, and absorption properties of crystalline furoxan under hydrostatic pressure of 0-160 GPa. The atomic positions and unit-cell parameters were allowed to relax to the minimum energy configuration to investigate the crystal structure at different pressures. Next we examined the structure changes under compression. Finally we discussed the pressure effects on the electronic and absorption properties.

2 Computational method

The calculations performed in this study were done within the framework of DFT based on CASTEP code [30], using Vanderbilt-type ultrasoft pseudopotentials [31] and a

RSC Advances Accepted Manuscript

plane-wave expansion of the wave functions. The self-consistent ground state of the system was determined by using a band-by-band conjugate gradient technique to minimize the total energy of the system with respect to the plane wave coefficients. The electronic wave functions were obtained using a density-mixing minimization method [32] for the self-consistent field calculation and the structures were relaxed using the Broyden, Fletcher, Goldfarb, and Shannon (BFGS) method [33]. Geometry optimization is based on reducing the magnitude of calculated forces and stresses until they become smaller than defined convergence tolerances. Therefore, it is possible to specify an external stress tensor to model the behavior of the system under tension, compression, shear, etc. In these cases the internal stress tensor is iterated until it becomes equal to the applied external stress. The LDA functional proposed by Ceperley and Alder [34] and parameterized by Perdew and Zunder [35], named CA-PZ, was employed. The dispersion-corrected DFT (DFT-D) approach by the Ortmann, Bechstedt, and Schmidt [36] for the LDA and GGA was used to treat vdW interactions. The cutoff energy of plane waves was set to 380 eV. Brillouin zones sampling was performed using the Monkhost-Pack scheme with a k-point grid of 3×3×2. The values of the kinetic energy cutoff and k-point grid were determined to ensure the convergence of total energies.

The enthalpies of the crystals at different pressures are calculated by eq. (1):

$$H = E_{tot} + PV \quad (1)$$

where E_{tot} is the total energy, P is the pressure, and V is the unit cell volume. The crystal structure of furoxan at ambient pressure and temperature was used as input

RSC Advances Accepted Manuscript

structure. The furoxan crystallizes in a monoclinic lattice with $P2_1/n$ space group and contains four $C_2H_2N_2O_2$ molecules per unit cell [4]. Fig. 1 displays crystal structure and atomic numbering of furoxan. The experimental crystal structure of furoxan[4] was first relaxed to allow the ionic configurations, cell shape, and volume to change at ambient pressure. Then from this relaxed structure, we applied hydrostatic compression of 1-160 GPa to relax the crystal structure without any symmetry constraints and the pressure is applied equally in all directions. All the calculations are based on the same crystal structure of furoxan. In the geometry relaxation, the total energy of the system was converged less than 2.0×10-5 eV, the residual force less than 0.05 eV/Å, the displacement of atoms less than 0.002 Å, and the residual bulk stress less than 0.1 GPa. Previous studies employed the same approach to simulate the hydrostatic compression of other organic molecular crystals [23, 28, 29, 37] indicate that the calculated results are in agreement with the experiments.

<Fig. 1 about here>

3 Results and discussion

3.1 Crystal and molecular structure

As a base and a benchmark for studying furoxan, both the LDA/CA-PZ and GGA/PW91 (Perdew-Wang 91) [38] with or without van der Waals [36] (vdW) corrections were applied to fully relax the bulk furoxan at ambient pressure without any constraints. Table 1 lists the experimental and optimized cell parameters of furoxan (S1). It is found that the errors of the LDA/CA-PZ results are smaller than those of the GGA/PW91 results. All the three lattice parameters are underestimated significantly

RSC Advances Accepted Manuscript

by the LDA+vdW [36]. The estimated *b* and *c* are close to the experimental values but *a* is overestimated obviously by the GGA+vdW [36]. In all, the LDA/CA-PZ results are most close to the experimental values, indicating that the LDA functional can produce more reliable crystal structures, which is in agreement with previous studies on organic molecular crystals [23, 39]. We also note in Table 2 that the internal structure parameters assigned by the LDA/CA-PZ bond lengths and angles are close to corresponding experimental data. The comparisons confirm that our computational parameters are reasonably satisfactory. Consequently, it is used in subsequent calculations.

<Table 1 and 2 about here>

Fig. 2 displays the perspective view of the unit cell of crystalline furoxan at different pressures. It can be seen that the crystal structure of furoxan at the pressures are different each other. When the pressure is increased from ambient pressure to 113 GPa, the crystal structure changes little except that the hydrogen atoms are out the plane of the ring to some degree. However, at 114 GPa, the length of one C-H bond increases suddenly and the hydrogen atom in this bond tends to transfer to the adjacent molecule to form a new C-H bond. This hydrogen transfer take place at 115 GPa and a new structure is formed (this new structure is denoted as S2). The S2 is still stable at 123 GPa. But when the pressure is increased to 124 GPa, another hydrogen transfers to form a new structure (denoted as S3) again. The S3 is stable until 135 GPa but transforms into a new structure (denoted as S4) which is caused by the polymerization of two adjacent furoxan molecules at 136 GPa. The structure S4 is still

RSC Advances Accepted Manuscript

stable at 160 GPa, which is the highest pressure investigated in this study. A simple changing process of the four structures is displayed in Fig. 3. Fig. 4 displays the perspective views of unimolecule in S1, S2, S3, and S4 from different viewpoints. First, the unimolecule in S1 has a planar conformation and all of the atoms in furoxan are approximately coplanar. Then, the unimolecule in S2 is also with a planar conformation approximately except that the two hydrogen atoms are above and below the plane, respectively. However, the unimolecule in S3 has a quite different conformation compared with that in S1 and S2, which can be named as a chair conformation approximately. Finally, the two rings in S4 are in the opposite positions and the unimolecule has a trans-conformation.

Fig. 5 displays the differences of the enthalpies (ΔH) of crystalline furoxan between different pressures and ambient pressure. It can be seen that ΔH decreases at 114 GPa and 115 GPa, which are caused by the occurrence of hydrogen transfer and the formation of S2. Then it also decreases irregularly both at 124 and 136 GPa, which are caused by the formation of S3 and S4, respectively. The enthalpy change of furoxan at different pressures supports our above-mentioned structural variations completely.

<Figs. 2, 3, 4 and 5 about here>

The relaxed lattice constants (*a*, *b*, *c*), unit cell angle, and unit cell volume of furoxan under different pressures are depicted in Fig. 6. First, *a*, *b*, and *c* change very irregularly at 114-115, 124, and 136 GPa with the formation of S2, S3, and S4, respectively. Then the formation of S2, S3, and S4 make the unit cell angle decrease

RSC Advances Accepted Manuscript

fast. Finally, the volume decreases obviously with the formation of S2 and S3, especially for the former, while the formation of S4 makes the volume increase significantly. The reason why S4 has larger volume than S3 may be that when S3 transforms into S4, two small molecules of S3 polymerizes to form one big molecule which leads to the significant increase of unimolecular volume. The formation of the big molecule can reduce the space utilization percentage obviously and so leads to the increase of unit cell volume.

<Fig. 6 about here>

Fig. 7 displays the bond lengths, bond angles, and torsion angle of furoxan under different pressures. By and large, the geometrical parameters change irregularly at 114-115, 124, and 136 GPa, which are caused by the formation of new structures through hydrogen transfers or polymerization. For instance, the C2-H3 bond length shortens from 2.00 to 1.16 Å, while the C1-H1 bond length elongates from 1.08 to 2.16 Å when the pressure is increased from 113 to 115 GPa. The C1-N1-O1 and C1-C2-N2 bond angles decrease about 9.0 ° and 7.2 ° at 124 GPa, respectively, while the C1-C2-N2-N1 torsion angle changes from -2.2 ° to -24.4 ° and from -24.5 ° to 0.4 °, respectively, when the pressure is increased from 123 to 124 GPa and from 135 to 136 GPa, respectively.

Overall, first, the furoxan undergoes a hydrogen transfer and forms a new structure (S2) with planar conformation approximately at 114-115 GPa. Then, it goes through another hydrogen transfer and forms the second new structure (S3) with a chair conformation at 124 GPa. Finally, it undergoes polymerization and forms the new

RSC Advances Accepted Manuscript

structure (S4) with a trans-conformation at 136 GPa.

<Fig. 7 about here>

3.2 Electronic structure

In this section, we turn to investigate the effects of pressure on the electronic structure by analyzing the variation trend of band structure and density of state (DOS) with the increasing pressure. Previous studies reported that the electronic band structure of organic molecular crystals have a great influence on their physical and chemical properties like impact sensitivity [27, 40-42]. Fig. 8 displays the band gaps of furoxan under different pressures using the LDA and GGA-PBE. It is found that the band gaps calculated by the GGA-PBE are slightly higher than those by the LDA, but the LDA and GGA-PBE present very similar pressure-induced variation trends. Thus, the results by the LDA are discussed here. In comparison with experiments, band gaps are generally underestimated in DFT calculations, but these errors are close to being shifts of band energies. Therefore, these band gaps are right qualitatively and are regarded as the lower limits.

First, furoxan is an insulator at ambient pressure because its band gap is more than 3 eV. But its band gap decreases to less than 2 eV when the pressure is increased to 60 GPa, indicating that it transforms into a semiconductor here. Then, the band gap decreases consistently until 123 GPa, especially at 115 GPa, where occurs a hydrogen transfer and forms a new structure S2. The band gap of S2 at 115 GPa is 0.07 eV, indicating that molecular crystal furoxan undergoes an electronic phase transition from a semiconductor to a metallic system due to the high degree of compression and

RSC Advances Accepted Manuscript

the formation of S2. When the pressure is increased from 123 to 124 GPa, its band gap increases from 0 eV to 2.8 eV with the formation of S3, indicating that S3 is a insulator. Finally, its band gap drops to 0 eV with the formation of S4 when the pressure is increased from 135 to 136 GPa, suggesting that furoxan transforms into a metal at 136 GPa. According to the first-principles band gap criterion of impact sensitivity [43] and some previous studies [31, 41, 42], it may be concluded that furoxan crystal becomes more and more sensitive with the reducing of band gap under compression. But it becomes much more insensitive at 124 GPa with the obvious increase of its band gap. Then, it becomes a little less sensitive when the pressure is increased till 135 GPa due to the slight increase of its band gap. Finally, it becomes greatly more sensitive at 136 GPa due to the decrease of its band gap to 0 eV. Thus, it may be inferred that S2 and S4 are much more sensitive than S1 and S3.

To understand the bond nature and electronic structure of furoxan at different pressures, we investigated its total density of states (TDOS) and partial density of states (PDOS). Fig. 9a displays the TDOS and PDOS of the C1 states (the C atom linked with NO), C2 states (the C atom linked with NOO), N1 states (the N atom linked with oxygen atom in the ring), N2 states (the N atom linked with two oxygen atoms), O1 states in the ring, and O2 states out of the ring of furoxan at 0 GPa. First, the PDOS peaks of these states in the valence band almost occur at the same energy. Thus, it can be expected that the adjacent atoms are bonded strongly and furoxan has good conjugation. Then, the PDOS of the C2 states, N1 states, and O2 states near the Fermi energy level are much larger than other states, suggesting that the C atom

RSC Advances Accepted Manuscript

linked with NOO, N atom with one oxygen atom, and O atom out of the ring may act as active centers. Finally, the PDOS of the six states in the conduction band are all two peaks and the peaks occur in the same energy. Fig. 9b depicts the DOS of furoxan under different pressures. First, the DOS at 115, 124, and 136 GPa are quite different with those at 113, 123, and 135 GPa, respectively, indicating that the structures of furoxan are changed completely at 115, 124, and 136 GPa. Then, the peaks become more and more wide and dispersed and have a tendency of shifting to the lower energy with the increasing pressure from 0 to 113 GPa, indicating that the band splitting and band dispersion increase accompanied by a broadening of DOS, which is caused by the increased intermolecular interactions under compression. Therefore, the electronic delocalization in bulk furoxan improves. Also, the DOS peaks join together near the Fermi energy level in the pressure range of 115-123 GPa and 136 GPa, indicating that furoxan has metallic character at the pressures. However, it becomes separated completely at this energy level in the pressure range of 124-135 GPa, suggesting that the electronic character of furoxan transforms from a metallic system to an insulator. This is in agreement with the results observed from the variation of the band gaps under compression.

<Fig.s 8 and 9 about here>

3.3 Elastic constants

To understand the mechanical stability of four different pressure-induced structures of furoxan, the elastic constants were calculated. It is known that the mechanical stability of crystal requires the strain energy to be positive, which implies that the whole set of

RSC Advances Accepted Manuscript

elastic constant C_{ij} satisfies the Born stability criterion. [44] And for the monoclinic phase crystal, the independent elastic stiffness tensor consists of thirteen components C_{11},C_{22}, C_{33}, C_{44}, C_{55}, C_{66}, C_{12}, C_{13}, C_{15}, C_{23}, C_{25}, C_{35}, and C_{46} in the Voigt notation. The Born stability criteria for monoclinic crystal are given as follows:

$$\begin{aligned}
&C_{ii} > 0, (i = 1,...,6), [C_{11} + C_{22} + C_{33} + 2(C_{12} + C_{13} + C_{23})] > 0 \\
&(C_{33}C_{55} - C_{35}^2) > 0, (C_{44}C_{66} - C_{46}^2) > 0, (C_{22} + C_{33} - 2C_{23}) > 0 \\
&[C_{22}(C_{33}C_{55} - C_{35}^2) + 2C_{23}C_{25}C_{35} - C_{23}^2C_{55} - C_{25}^2C_{33}] > 0 \\
&\{2[C_{15}C_{25}(C_{33}C_{12} - C_{13}C_{23}) + C_{15}C_{35}(C_{22}C_{13} - C_{12}C_{23}) + C_{25}C_{35}(C_{11}C_{23} - C_{12}C_{13})] \\
&-[C_{15}^2(C_{22}C_{33} - C_{23}^2) + C_{25}^2(C_{11}C_{33} - C_{13}^2) + C_{35}^2(C_{11}C_{22} - C_{12}^2)] + C_{55}g\} > 0 \\
&(g = C_{11}C_{22}C_{33} - C_{11}C_{23}^2 - C_{22}C_{13}^2 - C_{33}C_{12}^2 + 2C_{12}C_{13}C_{23})
\end{aligned} \tag{2}$$

The elastic constants of furoxan calculated at 0 GPa (S1), 115 GPa (S2), 124 GPa (S3), and 136 GPa (S4) by the LDA and GGA-PBE are listed in Table 3. It is found that all the elastic constants by the LDA and GGA satisfy the Born stability criteria [44], which suggesting that the four structures are mechanically stable. It is found that the results by the LDA and GGA are similar. Therefore, the results by the LDA are discussed here.

Fig. 10 displays the changing trend of elastic constants of furoxan under pressures. First, when S1 at 113 GPa transforms into S2 at 115 GPa, all of the elastic constants increase except for C35 which decreases obviously. The above behavior can be attributed to the increase of most of the C1-C2, C1-N1, N1-O1, and C2-C3 bond lengths and the formation of a new C2-H3 covalent bond. Then, when S2 at 123 GPa transforms into S3 at 124 GPa, some elastic constants (C11, C33, C23, C55, C44, C35, and C12) increase, while the others (C22, C44, C66, C15, and C25) decrease. This may be due to the decrease of some of the C2-N2 and C1-H4 bond lengths and the

RSC Advances Accepted Manuscript

increase of the C1-C2 and C2-H3 bond lengths. A similar changing trend can be seen when S3 at 135 GPa transforms into S4 at 136 GPa. It should be notable that S4 has much higher C35 than S3. This behavior can be attributed to the polymerization of furoxan and the formation of two C2-C3 and C1-C4 covalent bonds (as shown in Fig. 7). Overall, an analysis of elastic constants indicates that the three new structures are mechanically stable and their changing trends are in agreement with the results observed from the variation of the bond lengths under compression.

<Fig. 10 about here>

3.4 Optical absorption spectra

In this section, we turn to investigate the optical absorption coefficients of furoxan at different pressures. The interaction of a photon with the electrons in the system can result in transitions between occupied and unoccupied states. The spectra resulting from these excitations can be described as a joint density of states between the valence and conduction bands. The imaginary part $\varepsilon_2(\omega)$ of the dielectric function can be obtained from the momentum matrix elements between the occupied and unoccupied wave functions within the selection rules, and the real part $\varepsilon_1(\omega)$ of dielectric function can be calculated from imaginary part $\varepsilon_2(\omega)$ by Kramer-Kronig relationship. Absorption coefficient $\alpha(\omega)$ can be evaluated from $\varepsilon_1(\omega)$ and $\varepsilon_2(\omega)$ [45].

$$\alpha(\omega) = \sqrt{2}\omega\left(\sqrt{\varepsilon_1^2(\omega) + \varepsilon_2^2(\omega)} - \varepsilon_1(\omega)\right)^{1/2} \quad (3)$$

The absorption coefficients $\alpha(\omega)$ of furoxan at different pressures are shown in Fig. 11. The absorption spectra are active over various regions corresponding to the molecular or lattice structures of the individual material. The evolution pattern of

RSC Advances Accepted Manuscript

absorption spectra for furoxan at different pressures have an absorption band covering from 0 to 37.5 eV and more strong optical absorption from 2.5 to 25.0 eV. The magnitude of the absorption coefficients of the peaks allows an optical transition maybe due to excitons. This is since the large absorption coefficient would lead the material to absorb more energy and then increase the possibility of electron transition. It can be seen that the absorption spectra at 115, 124, and 136 GPa are totally different with those at 113, 123, and 135 GPa, respectively, indicating that furoxan undergoes huge changes in the structure at 115, 124, and 136 GPa, respectively. This agrees with the structural variation under compression. At ambient pressure, furoxan exhibits a relatively few, closely spaced bands with relatively high absorption coefficients. Four strong peaks are observed at 5.85, 11.06, 13.13, and 16.45 eV. In the energy below 3.19 eV or above 18.08 eV, the absorption coefficients are close to zero, indicating that furoxan is transparent in the wavelength range higher than 388 nm or lower than 68 nm. This suggests that the absorption regions of furoxan at ambient pressure are located in ultraviolet region. In the pressure range of 0-113 GPa, the absorption coefficients of several main peaks enhance consistently, indicating that furoxan has relatively high optical activity at high pressures. When the pressure is increased from 113 to 115 GPa, the absorption coefficients of main peaks are improved greatly, suggesting that S2 has much higher optical activity than S1. When the pressure is increased from 123 to 124 GPa, the absorption coefficients in the energy range of 7.9-24.0 eV (52-157 nm) are enhanced obviously, indicating that S3 has higher optical activity than S2 in far ultraviolet region. But the absorption coefficients below 7.8 eV

RSC Advances Accepted Manuscript

at 124 GPa are lower than that at 123 GPa obviously and the absorption coefficients below 2.5 eV is zero at 124 GPa, indicating that S3 narrows the absorption range down to near ultraviolet, visible, and infrared light region compared with S2. When the pressure is increased from 135 to 136 GPa, the absorption coefficients in the energy range of 7.3-27.5 eV (45-170 nm) decrease significantly, suggesting that S4 has much weaker optical activity than S3 in far ultraviolet region. But the absorption coefficients of S4 below 7.2 eV (172 nm) are higher than those of S3, indicating that S4 broadens the absorption range to near ultraviolet, visible, and infrared light region compared with S3. The absorption coefficients of S4 are close to those of S2 in all energy range, indicating that S4 and S2 have comparative optical activity.

In all, furoxan has relatively high optical activity at high pressures in the range of 0-113 GPa. S2 has higher optical activity than S1. S3 has higher optical activity than S2 in far ultraviolet region, but it narrows the absorption range down to near ultraviolet, visible, and infrared light region. S4 has weaker optical activity than S3 in far ultraviolet region, but it broadens the absorption range to near ultraviolet, visible, and infrared light region. S4 and S2 have comparative optical activity. The differences in optical activity are caused by different structural transformations under pressures.

<Fig. 11 about here>

4 Conclusions

In this work, DFT calculations have been performed to study the structural transformations, electronic structure, elastic constants, and absorption properties of crystalline furoxan (S1) under hydrostatic compression of 0-160 GPa. The results

RSC Advances Accepted Manuscript

show that furoxan undergoes a hydrogen transfer to form a new structure (S2) with approximate planar conformation at 114-115 GPa first. Then, it goes through another hydrogen transfer and forms the second new structure (S3) with chair conformation at 124 GPa. Finally, it undergoes polymerization and forms another new structure (S4) with a trans-conformation at 136 GPa. Both hydrogen transfers and polymerization make the geometrical parameters change irregularly.

An analysis of its band gap and density of states under compression indicates that it becomes more and more sensitive and its electronic delocalization is improved in the pressure of 0-113 GPa. The first hydrogen transfer occurs at 114-115 GPa makes it transform from a semiconductor into a metal. The second hydrogen transfer at 124 GPa makes it change to a insulator. The polymerization at 136 GPa makes it undergo a transition from a insulator to a metal.

The calculated elastic constants indicate that the three new structures are mechanically stable and their changing trends are in agreement with the results observed from the variation of the band lengths under compression. Its absorption spectra show that it has relatively high optical activity at high pressure in the range of 0-113 GPa. S2 has higher optical activity than S1. S3 has higher optical activity than S2 in far ultraviolet region, but it narrows the absorption range down to near ultraviolet, visible, and infrared light region. S4 has weaker optical activity than S3 in far ultraviolet region, but it broadens the absorption range to near ultraviolet, visible, and infrared light region.

This work may provide useful information in understanding how furoxan behaves

RSC Advances Accepted Manuscript

under high pressure and may be helpful for understanding some new structures that are not observed at the ambient conditions.

Acknowledgments

This work was supported by the National Natural Science Foundation of China (Grant No. 21273115) and A Project Funded by the Priority Academic Program Development of Jiangsu Higher Education Institutions. Q.W. thanks the Innovation Project for Postgraduates in Universities of Jiangsu Provi nce (Grant No. CXZZ13_0199) for partial financial support.

References

1 B. T. Federoff, Encyclopedia of Explosives and Related Items; Picatinny Arsenal: Dover, NJ, 1962.
2 Y. Oyumi and T. B. Brill, *Combust. Flame*, 1986, **65**, 313-318.
3 B. M. Rice and J. J. Hare, *J. Phys. Chem. A*, 2002, **106**, 1770-1783.
4 T. I. Godovikova, S. P. Golova, Y. A. Strelenko M. Yu., Antipin, Y. T. Struchkov and L. I. Khmel'nitskii, *Mendeleev Commun.*, 1994, **4**, 7-9.
5 V. I. Kovalenko, V. L. Furer, L. I. Anisimova and E. M. Yagund, *J. Struct. Chem.*, 1994, **35**, 799-803.
6 T. Pasinszki, B. Havasi, B. Hajgató and N. P. C. Westwood, *J. Phys. Chem. A*, 2009, **113**, 170-176.
7 E. Sedano, C. Sarasola, J. M. Ugalde, I. X. Irazabalbeita and A. G. Guerrero, *J. Phys. Chem.*, 1988, **92**, 5094-5096.
8 J. M. Seminario, M. C. Concha and P. Politzer, *J. Comput. Chem.*, 1992, **13**, 177-182.
9 G. Rauhut and H. J. Werner, *Phys. Chem. Chem. Phys.*, 2003, **5**, 2001-2008.
10 J. Stevens, M. Schweizer and G. Rauhut, *J. Am. Chem. Soc.*, 2001, **123**, 7326-7333.
11 H. H. Cady, A. C. Larson and D. T. Cromer, *Acta Cryst.*, 1966, **20**, 336-341.
12 B. H. L. Ammon and S. K. Bhattacharjee, *Acta Cryst.*, 1982, **B38**, 2498-2602.
13 H. H. Cady and L. C. Smith, *Los Alamos Scientific Laboratory Repot LAMS-2653 TID-4500*, Los Almos National Laboratory, Los Alamos, NM, 1961.
14 P. Main, R. E. Cobbledic and R. W. H. Small, *Acta Crystallogr.*, *Sect. C*, 1985, **41**, 1351-1354.
15 Z. A. Dreger and Y. M. Gupta, *J. Phys. Chem. A*, 2010, **114**, 8099-8105.
16 M. B. Matthew, S.C. Raja, P. Michael, C. Josh and Z.X. Liu, *J. Chem. Phys.*, 2012,

RSC Advances Accepted Manuscript

137, 174304.
17 Z. A. Dreger and Y. M. Gupta, *J. Phys. Chem. A*, 2007, **111**, 3893-3903.
18 S. R. Rice and M. F. Foltz, *Combust. Flame*, 1991, **87**, 109-122.
19 M. F. Foltz, *Propell. Explos. Pyrot.*, 1993, **18**, 210-216.
20 B. Olinger, P. M. Halleck and H. H. Cady, *J. Chem. Phys.*, 1975, **62**, 4480-4483.
21 K. E. Lipinska-Kalita, M. G. Pravica and M. Nicol, *J. Phys. Chem. B*, 2005, **109**, 19223-19227.
22 R. J. Hemley, *Annu. Rev. Phys. Chem.*, 2000, **51**, 763-800.
23 Q. Wu, W.H. Zhu, H.M. Xiao, *J. Phys. Chem. C*, 2013, **117**, 16830-16839.
24 B. M. Rice and D. C. Sorescu, *J. Phys. Chem. B*, 2004, **108**, 17730-17739.
25 W. H. Zhu, J. J. Xiao and H. M. Xiao, *Chem. Phys. Lett.*, 2006, **422**, 117-121.
26 W. H. Zhu and H. M. Xiao, *J. Phys. Chem. B*, 2006, **110**, 18196-18203.
27 W. H. Zhu and H. M. Xiao, *J. Comput. Chem.*, 2008, **29**, 176-184.
28 E. F. C. Byrd and B. M. Rice *J. Phys. Chem. C*, 2007, **111**, 2787-2796.
29 W. H. Zhu, X. W. Zhang, T. Wei and H. M. Xiao, *Theor. Chem. Acc.*, 2009, **124**, 179-186.
30 M. D. Segall, P. J. D. Lindan, M. J. Probert, C. J. Pickard, P. J. Hasnip, S. J. Clark and M. C. Payne, *J. Phys. Condens. Matter.*, 2002, **14**, 2717-2744.
31 D. Vanderbilt, *Phys. Rev. B*, 1990, **41**, 7892-7895.
32 G. Kresse and J. Furthmüller, *Phys. Rev. B*, 1996, **54**, 11169-11186.
33 R. Fletcher, *Practical Methods of Optimization vol 1*, Wiley, New York, 1980.
34 D. M. Ceperley and B. J. Alder, *Phys. Rev. Lett.*, 1980, **45**, 566-569.
35 J. P. Perdew and A. Zunger, *Phys. Rev. B*, 1981, **23**, 5048-5079.
36 F. Ortmann, F. Bechstedt and W. G. Schmidt, *Phys. Rev. B*, 2006, **73**, 205101
37 Q. Wu, W. H. Zhu and H. M. Xiao, *J. Mol. Model.*, 2013, **19**, 4039-4047.
38 J. P. Perdew, J. A. Chevary, S. H. Vosko, K. A. Jackson, M. R. Pederson, D. J. Singh and C. Fiolhais, *Phys. Rev. B*, 1992, **46**, 6671-6687.
39 Q. Wu, W. H. Zhu and H. M. Xiao, *Comput. Theor. Chem.*, 2014, **1030**, 38-43.
40 W. H. Zhu, J. J. Xiao, G. F. Ji, F. Zhang and H. M. Xiao *J. Phys. Chem. B*, 2007, **111**, 12715-12722.
41 J. J. Gilman, *Philos. Mag. Lett.*, 1998, **77**, 79-82.
42 T. Luty, P. Ordon and C. J. Eckhardt, *J. Chem. Phys.*, 2002, **117**, 1775-1785.
43 W. H. Zhu and H. M. Xiao, *Struct. Chem.*, 2010, **21**, 657-665.
44 M. Born and K. Huang, Dynamical Theory of Crystal Lattices, Clarendon, Oxford, 1956.
45 S. Saha, T. P. Sinha and A. Mookerjee, *Phys. Rev. B*, 2000, **62**, 8828-8834.

RSC Advances Accepted Manuscript

Fig. 1 The crystal structure and atomic numbering of furoxan (S1).

Fig. 2 The perspective view of the unit cell of furoxan at different pressures.

Fig. 3 A simple variation process of S1, S2, S3, and S4.

Fig. 4 The perspective views of the unimolecule in S1, S2, S3, and S4 from different viewpoints.

Fig. 5 The differences of the enthalpies of furoxan between different pressures and ambient pressure.

Fig. 6 The relaxed lattice constants (*a*, *b*, *c*), unit cell angle, and unit cell volume of furoxan under different pressures.

Fig. 7 The bond lengths, bond angles, and torsion angle of furoxan under different pressures.

Fig. 8 The band gaps of furoxan under different pressures by the LDA and GGA-PBE.

Fig. 9 Total and partial density of states (DOS) of furoxan under different pressures. The Fermi energy is shown as a vertical dashed line.

Fig. 10 The elastic constants of furoxan under different pressures.

Fig. 11 The absorption coefficients $\alpha(\omega)$ of furoxan under different pressures.

Table 1. Comparison of optimized lattice parameters for furoxan with experimental

RSC Advances Accepted Manuscript

data at ambient pressure [a, b]

	a(Å)	*b*(Å)	*c*(Å)	β(°)	cell volume
Expt.	8.249	5.004	8.675	104.72	346.3
LDA/CA-PZ	7.955(-3.6)	5.017(0.3)	9.090(4.8)	105.94(1.2)	348.8(0.7)
LDA/CA-PZ+vdW	7.437(-9.8)	4.565(-8.8)	8.300(-4.3)	101.67(-2.9)	275.9(-20.3)
GGA/PW91	8.720(5.7)	5.320(6.3)	9.187(5.9)	106.78(2.0)	408.1(17.8)
GGA/PW91+vdW	8.852(7.3)	5.090((1.7)	8.695(0.2)	107.04(2.2)	374.5(8.1)

[a] Values in parentheses correspond to the percentage differences relative to the experimental data. [b] The vdW corrections by the Ortmann, Bechstedt, and Schmidt [36] to the LDA/CA-PZ and GGA/PW91 were used.

Table 2. Calculated and experimental bond lengths (Å) and bond angles (°) for furoxan.

	LDA	Expt.		LDA	Expt.
C1-C2	1.398	1.402	C1-C2-N2	111.1	111.8
C2-N2	1.314	1.292	C2-N2-O1	107.6	106.6
N1-C1	1.320	1.302	N1-O1-N2	107.5	107.1
N1-O1	1.474	1.441	H2-C2-N1	162.6	163.2
N1-O2	1.244	1.240	O2-N1-C2	173.3	174.3
O1-N2	1.352	1.379	C1-C2-N2-N1	-0.04	0.20

Table 3. The calculated elastic constants (GPa) of S1 at 0 GPa, S2 at 115 GPa, S3 at

RSC Advances Accepted Manuscript

124 GPa, and S4 at 136 GPa.

P (GPa)		C_{11}	C_{22}	C_{33}	C_{44}	C_{55}	C_{66}	C_{12}	C_{13}	C_{15}	C_{23}	C_{25}	C_{35}	C_{46}
0	GGA	18.8	22.9	16.0	5.3	5.1	8.1	12.8	10.6	1.7	9.7	-3.1	3.9	0.9
	LDA	9.0	4.3	-0.8	4.8	-2.9	2.1	4.7	-1.6	-1.1	-1.5	5.0	-1.1	1.7
115	GGA	708.0	1732.8	746.2	209.6	312.3	320.5	345.1	516.7	52.2	308.9	127.5	-44.8	222.1
	LDA	722.5	1702.9	767.4	211.5	306.7	324.5	340.9	466.4	71.2	294.7	133.9	-53.1	208.9
124	GGA	843.3	1453.8	826.4	348.2	352.9	306.4	391.8	450.8	-12.9	367.1	79.3	16.5	121.2
	LDA	792.1	1429.5	812.7	333.2	340.0	308.2	367.7	427.2	-9.4	338.6	96.0	23.4	117.7
136	GGA	960.1	853.9	914.4	195.4	211.8	203.0	432.4	480.7	35.4	492.8	-173.5	198.3	105.7
	LDA	923.4	878.2	920.0	178.9	262.7	213.6	455.0	452.7	37.0	461.2	-88.2	157.4	66.5

RSC Advances Accepted Manuscript

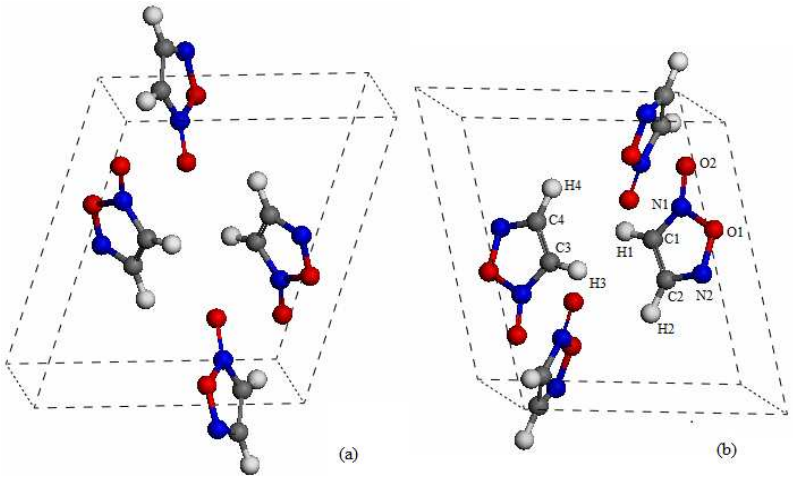

Fig. 1 The crystal structure and atomic numbering of furoxan (S1).

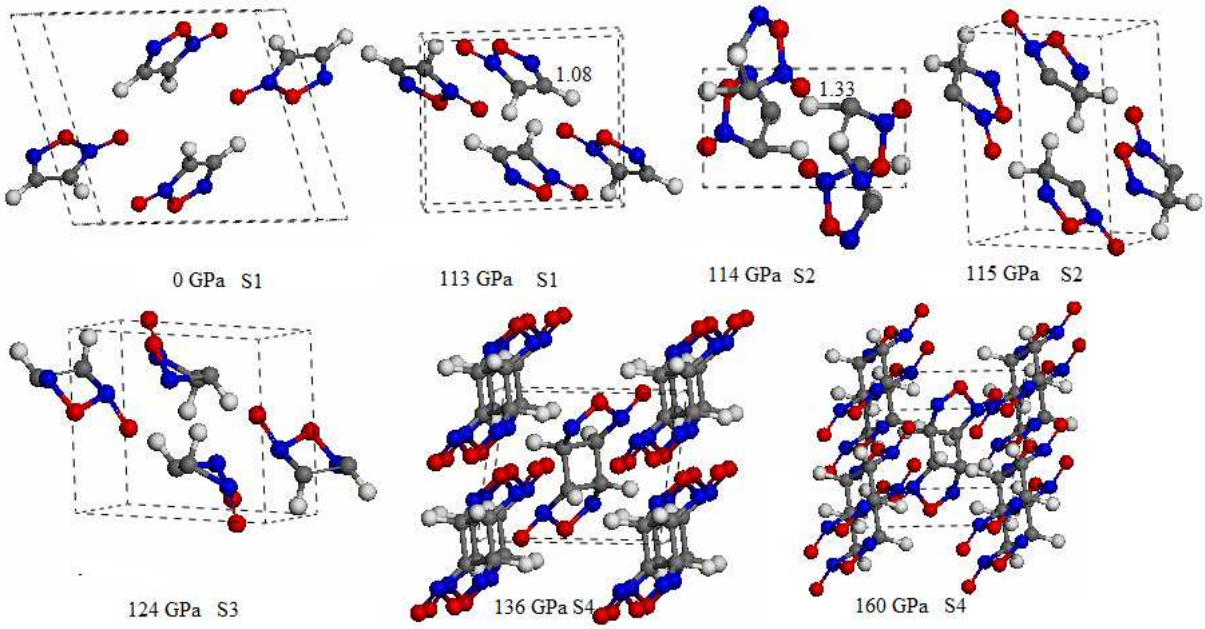

Fig. 2 The perspective views of the unit cell of furoxan at different pressures.

RSC Advances Accepted Manuscript

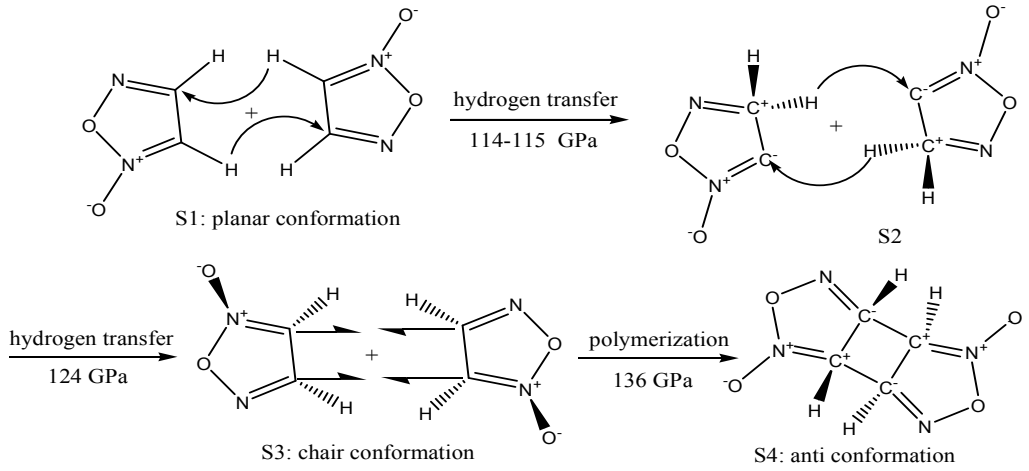

Fig. 3 A simple variation process of S1, S2, S3, and S4.

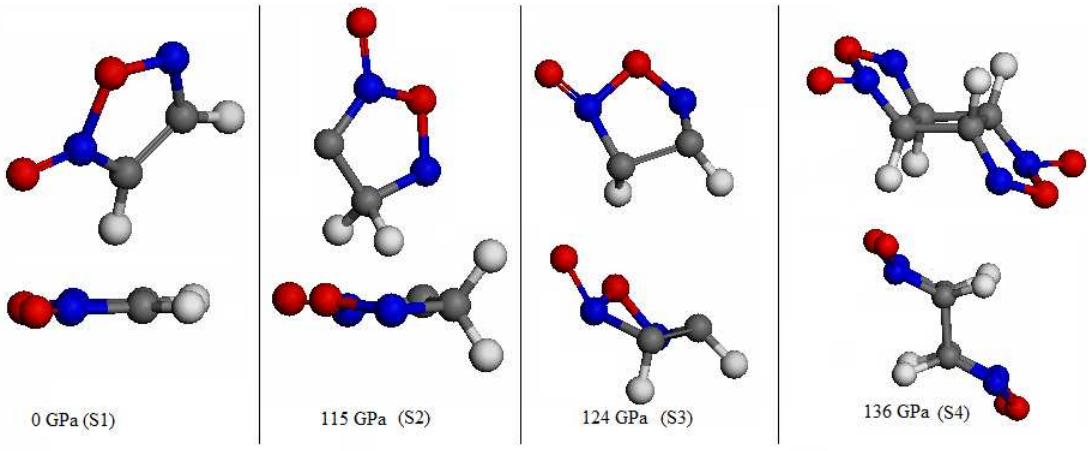

Fig. 4 The perspective views of the unimolecule in S1, S2, S3, and S4 from different viewpoints.

RSC Advances Accepted Manuscript

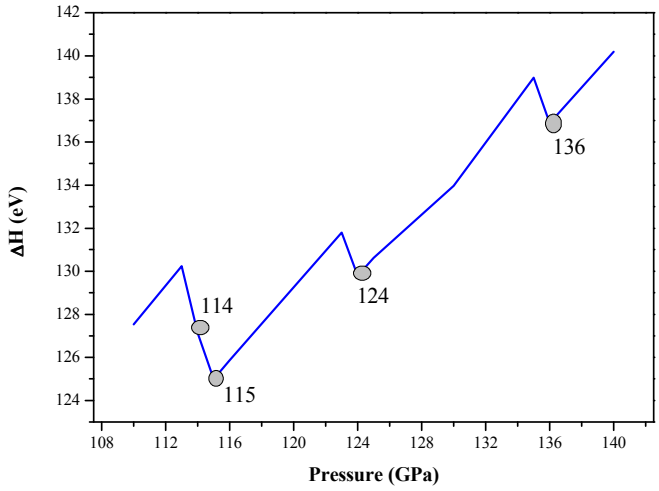

Fig. 5 The differences of the enthalpies of furoxan between different pressures and ambient pressure.

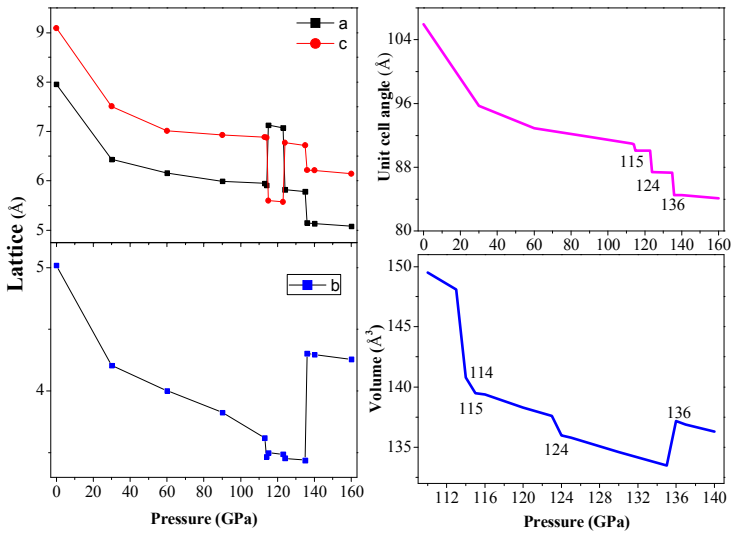

Fig. 6 The relaxed lattice constants (*a*, *b*, *c*), unit cell angle, and unit cell volume of furoxan crystal under different hydrostatic pressures.

RSC Advances Accepted Manuscript

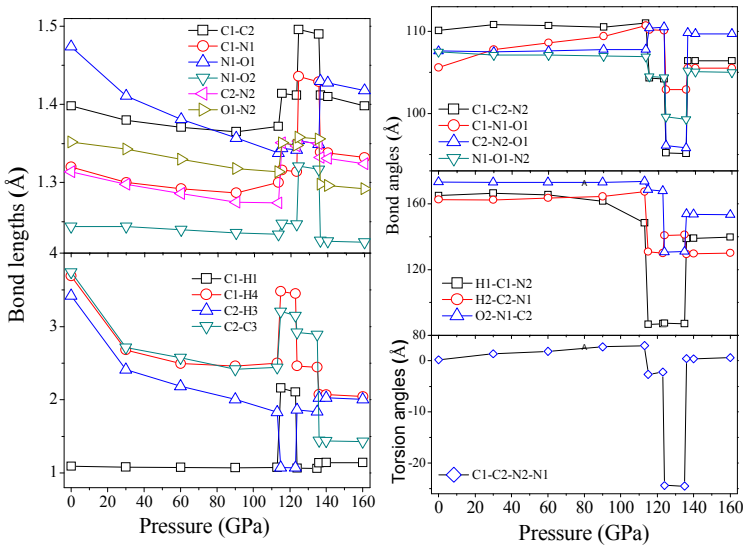

Fig. 7 The bond lengths, bond angles, and torsion angle of furoxan under different pressures.

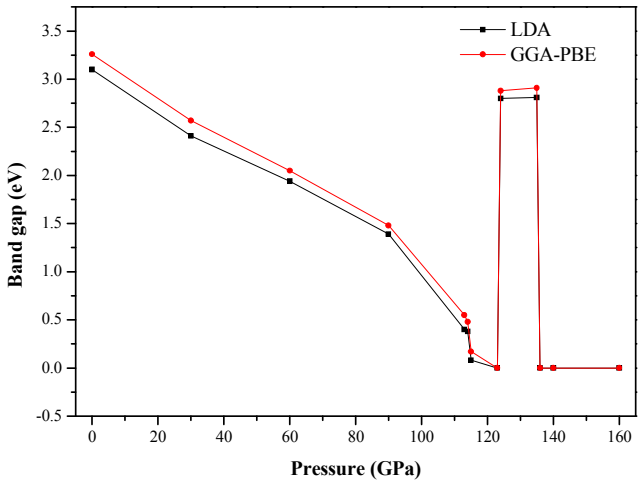

Fig. 8 The band gaps of furoxan under different pressures by the LDA and GGA-PBE.

RSC Advances Accepted Manuscript

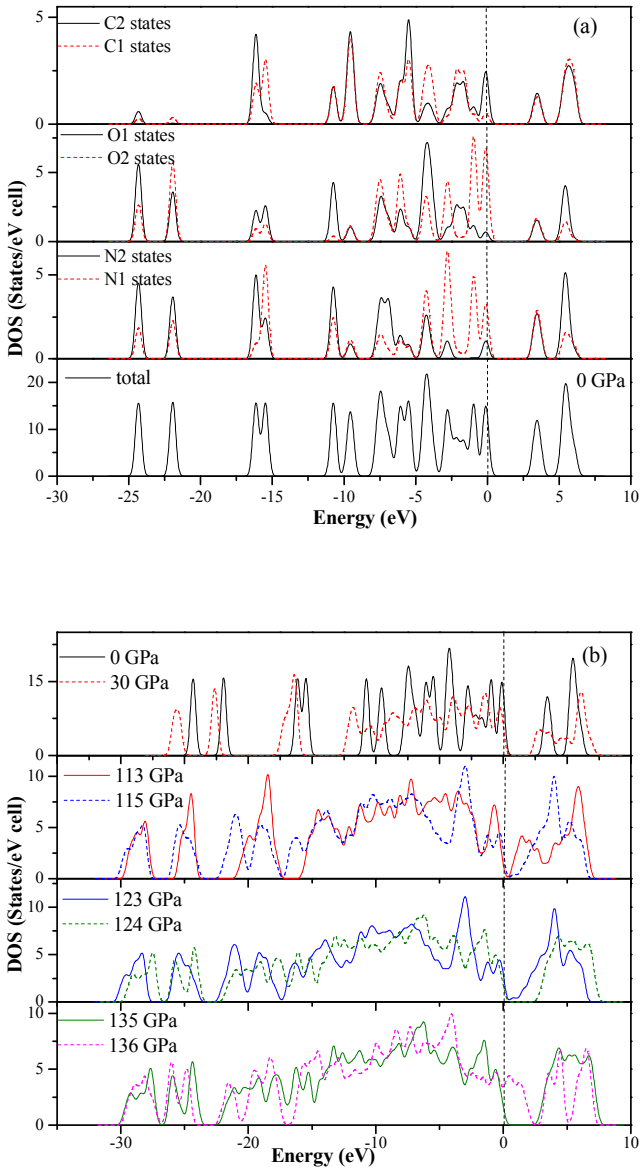

Fig. 9 Total and partial density of states (DOS) of furoxan under different pressures.

The Fermi energy is shown as a vertical dashed line.

RSC Advances Accepted Manuscript

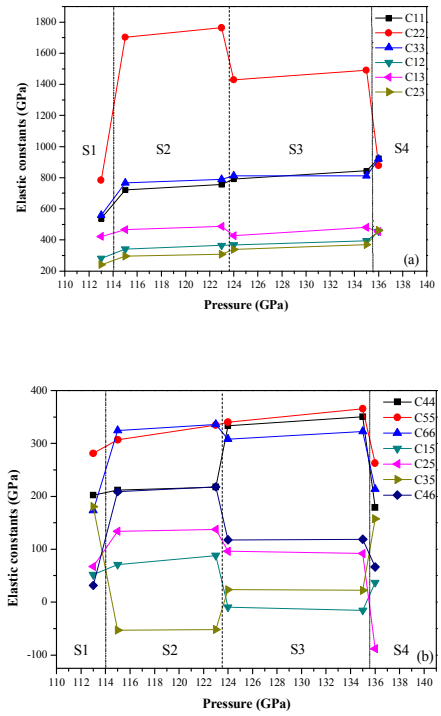

Fig. 10 The elastic constants of furoxan under different pressures.

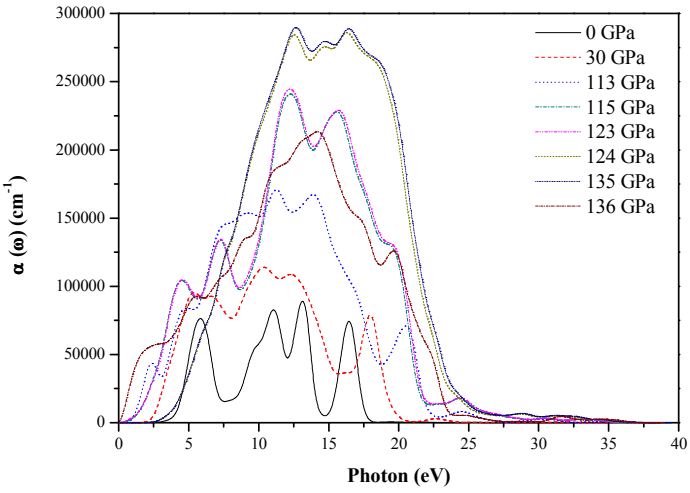

Fig. 11 The absorption coefficients α(ω) of furoxan under different pressures.

RSC Advances Accepted Manuscript

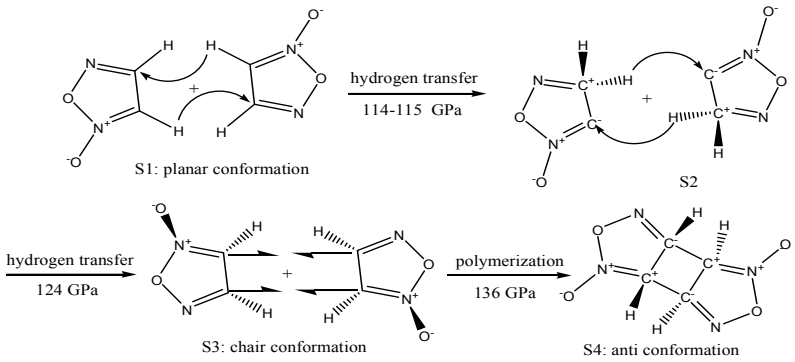

Under compression, furoxan (S1) transforms to S2, then forms S3 with chair conformation, and finally becomes S4 with a trans-conformation.

RSC Advances Accepted Manuscript